



Published in final edited form as:

Cell Rep. 2017 December 26; 21(13): 3728–3739. doi:10.1016/j.celrep.2017.11.100.

RNA-Independent DNA Cleavage Activities of Cas9 and Cas12a

Ramya Sundaresan^{1,2}, Hari Priya Parameshwaran^{1,2}, S.D. Yogesha^{1,3}, Mark Walter Keilbarth^{1,4}, and Rakhi Rajan^{1,5,*}

¹Department of Chemistry and Biochemistry, Stephenson Life Sciences Research Center, University of Oklahoma, 101 Stephenson Parkway, Norman, OK 73019, USA

SUMMARY

CRISPR-Cas systems provide bacteria and archaea with sequence-specific protection against invading mobile genetic elements. In the presence of divalent metal ions, Cas9 and Cas12a (formerly Cpf1) proteins target and cleave DNA that is complementary to a cognate guide RNA. The recognition of a protospacer adjacent motif (PAM) sequence in the target DNA by Cas9 and Cas12a is essential for cleavage. This RNA-guided DNA targeting is widely used for gene-editing methods. Here, we show that *Francisella tularensis novicida* (Fno) Cas12a, FnoCas9, and *Streptococcus pyogenes* Cas9 (SpyCas9) cleave DNA without a guide RNA in the presence of Mn²⁺ ions. Substrate requirements for the RNA-independent activity vary. FnoCas9 preferentially nicks double-stranded plasmid, SpyCas9 degrades single-stranded plasmid, and FnoCas12a cleaves both substrates. These observations suggest that the identities and levels of intracellular metals, along with the Cas9/Cas12a ortholog employed, could have significant impacts in genome editing applications

In Brief

This is an open access article under the CC BY-NC-ND license (<http://creativecommons.org/licenses/by-nc-nd/4.0/>).

*Correspondence: r-rajan@ou.edu.

²These authors contributed equally

³Present address: Cytovance Biologics, 800 Research Parkway, Suite 200, Oklahoma City, OK 73104, USA

⁴Present address: St. John Medical Center, 1923 South Utica Avenue, Tulsa, OK 74104, USA

⁵Lead Contact

SUPPLEMENTAL INFORMATION

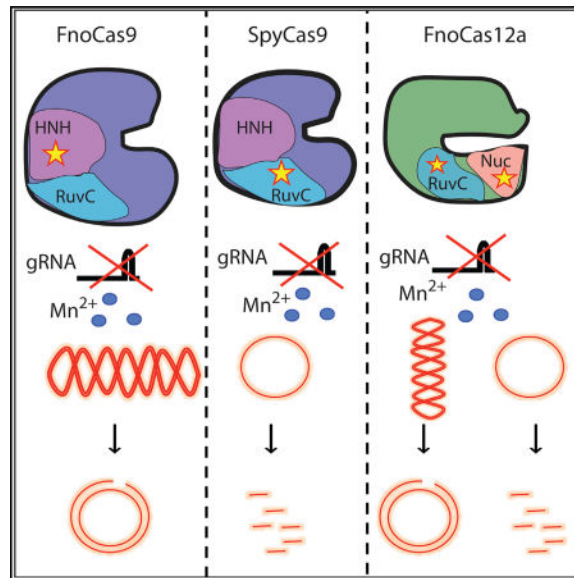
Supplemental Information includes Supplemental Experimental Procedures, seven figures, and four tables and can be found with this article online at <https://doi.org/10.1016/j.celrep.2017.11.100>.

AUTHOR CONTRIBUTIONS

S.D.Y. and R.R. conceived the idea; R.S., H.P.P., S.D.Y., and R.R. designed experiments; S.D.Y. constructed strains; R.S., S.D.Y., and H.P.P. expressed and purified proteins; R.S., S.D.Y., H.P.P., M.W.K., and R.R. performed experiments; R.S., H.P.P., S.D.Y., and R.R. analyzed data; R.S., H.P.P., and R.R. wrote the manuscript; and all authors edited the manuscript.

DECLARATION OF INTERESTS

The authors have no financial or other competing interests to declare.



CRISPR-mediated gene editing involves DNA targeting using complementary guide RNAs (gRNAs). Sundaresan et al. find that Cas9/Cas12a orthologs cause RNA-independent, non-sequence-specific DNA cleavage in the presence of Mn²⁺ ions. These observations suggest that the type of Cas9/Cas12a and levels of intracellular metal ions may affect CRISPR-based genome editing.

INTRODUCTION

CRISPR and Cas constitute an RNA-based immune system present in bacteria and archaea. CRISPR systems render sequence-specific inactivation of foreign nucleic acid (DNA and/or RNA) entering the cell (Barrangou et al., 2007; Brouns et al., 2008; Hale et al., 2009; Jansen et al., 2002; Marraffini and Sontheimer, 2008). The CRISPR-Cas defense mechanism records a cell's encounters with foreign DNA and/or RNA and provides adaptive immunity against future attacks by the same material (Barrangou et al., 2007; Gasiunas et al., 2012).

The CRISPR locus consists of a *cas* operon and a CRISPR array, coding for the Cas proteins and CRISPR RNA (crRNA), respectively. The CRISPR array consists of unique non-repetitive sequences derived from foreign genetic elements, spacers, that are interspersed between short repetitive sequences, repeats (Brouns et al., 2008; Ishino et al., 1987; Jansen et al., 2002; Mojica et al., 2005). The CRISPR defense mechanism includes three stages: (1) adaptation, in which spacers are acquired; (2) crRNA biogenesis that produces a guide RNA; and (3) target interference, in which a Cas protein catalyzes site-specific cleavage of the foreign nucleic acid complementary to the crRNA (Jinek et al., 2012; Wright et al., 2016). Many CRISPR systems require a short 2- to 7-nucleotides (nt)-long protospacer adjacent motif (PAM) (Mojica et al., 2005, 2009) in the intruder DNA to distinguish between self and non-self targets (Jinek et al., 2012), while other systems distinguish through crRNA-target base-pairing patterns (Marraffini and Sontheimer, 2010).

The CRISPR-Cas systems are grouped into two classes that are further divided into several types (I–VI) and sub-types based on the architecture of the CRISPR-Cas locus (Koonin et al., 2017). Cas9, the signature protein of the type II CRISPR system, requires crRNA, along with a *trans*-activating crRNA (tracrRNA), to achieve DNA interference (Garneau et al., 2010; Gasiunas et al., 2012; Jinek et al., 2012). Type II-A (a sub-type of type II) *Streptococcus pyogenes* Cas9 (SpyCas9) is the most functionally and structurally characterized ortholog (Jiang et al., 2015, 2016; Jinek et al., 2012, 2014; Nishimasu et al., 2014), and it has been widely used for gene-editing applications since its initial success in mammalian cells (Cong et al., 2013; Jinek et al., 2013; Mali et al., 2013; Wang et al., 2013). The crystal structures of other Cas9-nucleic acid complexes from *Francisella tularensis novicida* (Fno) (Hirano et al., 2016), *Staphylococcus aureus* (Nishimasu et al., 2015), and *Campylobacter jejuni* (Cje) (Yamada et al., 2017) also provide insights into the similarities and divergences of CRISPR-Cas9 systems. Cas12a (formerly called Cpf1), the signature protein for the type V-A CRISPR system, cleaves DNA guided by crRNA without an accompanying tracrRNA (Zetsche et al., 2015). Unlike Cas9, Cas12a is also known to cleave precursor crRNA during crRNA biogenesis (Fonfara et al., 2016). The crystal structures of Cas12a in complex with crRNA and/or DNA have provided structural insights into the mechanism of DNA cleavage (Dong et al., 2016; Gao et al., 2016; Swarts et al., 2017; Yamano et al., 2016).

Cas9 and Cas12a possess similarities and differences in their DNA cleavage mechanisms. Cas9 uses the HNH domain to cleave the DNA strand complementary to the crRNA sequence and the RuvC domain to cleave the DNA strand that is non-complementary to crRNA (Gasiunas et al., 2012; Jinek et al., 2012). Cas12a possesses a RuvC domain and a Nuclease (Nuc) domain (Gao et al., 2016; Yamano et al., 2016). The RuvC domain of Cas12a cleaves both the non-complementary and the complementary strands of the double-stranded DNA (dsDNA), while the Nuc domain assists in the cleavage process (Swarts et al., 2017; Yamano et al., 2016). Active site mutations in the RuvC and HNH domains convert the Cas9-crRNA complex into a strand-specific nicking endonuclease (Gasiunas et al., 2012; Jinek et al., 2012), whereas mutations in the RuvC domain of Cas12a abolish cleavage of both DNA strands (Yamano et al., 2016).

Even though dual RNAs (crRNA and tracrRNA) and a PAM region are essential for Cas9-mediated dsDNA cleavage, several type II-C Cas9 proteins cleave single-stranded DNA (ssDNA) that lacks a PAM using only crRNA as a guide (Ma et al., 2015; Zhang et al., 2015). Cas9 was shown to cut ssDNA bound to the crRNA using its HNH active site. A study reported that unexpected mutations were observed in the genomes of mice that were edited using CRISPR-Cas9 compared to a non-edited control mouse (Schaefer et al., 2017), though further studies are necessary to corroborate this conclusion. Nonetheless, these results emphasize the need for further characterization of the DNA cleavage mechanisms of CRISPR-Cas systems, particularly in understanding their potential activities and effects within the complex cellular environment.

Here, our studies demonstrate that FnoCas9, SpyCas9, and FnoCas12a possess RNA-independent, non-sequence-specific cleavage activities on dsDNA and ssDNA targets in the presence of Mn²⁺. While FnoCas12a and FnoCas9 possess an RNA-independent double-

stranded (ds) plasmid nicking activity, FnoCas12a and SpyCas9 catalyze ssDNA degradation. In FnoCas9, the HNH domain is responsible for the nicking activity, while in SpyCas9, the RuvC domain degrades the ssDNA. In FnoCas12a, the coordinated activity of the RuvC and the Nuc domains are essential for both DNA cleavage activities. These observations emphasize the need for caution in genome editing depending on the type of Cas9/Cas12a ortholog that is being used.

RESULTS

Cas9 Orthologs and Cas12a Possess RNA-Independent DNA Cleavage Activities

Our sequence analyses of Cas12a showed similarities to SbcC, a protein that belongs to the structural maintenance of chromosomes (SMC) family of proteins essential for DNA break repair, cell division, and other pathways. It associates with SbcD, an enzyme that possesses ATP-dependent nuclease activity in the presence of Mn^{2+} (Kamble and Misra, 2010). We tested the ability of purified, recombinant FnoCas12a to cleave ds plasmid (pUC19) in the presence of Mn^{2+} and ATP, without the addition of exogenous RNA. We observed plasmid cleavage with ATP- Mn^{2+} , and this cleavage was not detectable with ATP- Mg^{2+} (Figure S1A). Further experiments showed that the plasmid cleavage requires only Mn^{2+} , not ATP (Figure 1). To determine the nature of the DNA cleavage, the plasmid was linearized with EcoRI (one site) or nicked with Nt.BspQI (one site) to generate mobility standards. The FnoCas12a produced a band that migrated similarly to the nicked plasmid, indicating that FnoCas12a can nick dsDNA in the presence of Mn^{2+} without an added guide RNA (Figure 1A). With this observation, we tested the ability of FnoCas9 and SpyCas9 for similar Mn^{2+} -dependent dsDNA cleavage activity in the absence of a guide RNA. We found that FnoCas9 nicks ds plasmid (Figure 1B), while SpyCas9 does not (Figure 1C). A cleavage assay conducted using pET28m plasmid showed similar results (Figures S1B and S1C).

We proceeded to analyze whether the RNA-independent, Mn^{2+} -dependent dsDNA cleavage extends to ssDNA. While FnoCas12a and SpyCas9 degraded circular ssDNA (M13mp18) in an RNA-independent manner, FnoCas9 showed minimal activity (Figures 1D and 1E). To further ensure that the RNA-independent DNA cleavage activity observed was not an artifact of our protein preparation, we performed our activity assays with a commercially available SpyCas9 from New England Biolabs (NEB-SpyCas9) (Figure S1D). NEB-SpyCas9 also possesses RNA-independent ssDNA degradation in the presence of Mn^{2+} , similar to what was observed using the SpyCas9 purified in our laboratory (Figures 1D and S1D). NEB-SpyCas9 did not nick ds plasmid, similar to the laboratory-purified SpyCas9.

Kinetics of RNA-Independent DNA Cleavage

To determine the robustness of the RNA-independent activity, we performed time course assays with the different substrates (Figure 2). The RNA-independent activity ranged from 50% to 80% of ds plasmid nicking and >90% of circular ssDNA degradation within a 30-min incubation period, depending on the protein preparation. FnoCas12a produces some linear DNA, along with the nicked DNA (Figure 2A). Linearization is incomplete after an overnight reaction, indicating that linearization likely results from the plasmid being nicked multiple times at nearby sites. We also observe that linearization increases when the amount

of protein in the reaction is increased (data not shown). FnoCas9 produces little or no linear product (Figure 2B). FnoCas12a and SpyCas9 are robust in degrading circular ssDNA, because around 80% of the substrate is degraded within the first 5 min of incubation (Figures 2C–2E). There is no accumulation of intermediate products during the circular ssDNA cleavage within the time points that were analyzed.

RNA-Independent DNA Cleavage Activities Are Not Due to Co-purified Cellular RNAs

To rule out the contribution of fortuitously co-purified RNA in the Mn^{2+} -dependent plasmid cleavage, we analyzed our protein preparations for RNA. A representative gel showing the purity of the recombinant proteins is presented in Figure S2A. Protein, RNA, and ribonucleoprotein (RNP) samples were passed through a size-exclusion column with simultaneous detection of absorbance at 254, 260, and 280 nm (Figures S2B and S2C). The same amount of protein was used in both protein and RNP samples to differentiate absorbance changes coming from RNA. The absorbance pattern for protein standards and RNA is shown for comparison (Figure S2B). The 260:280 nm ratio for the protein shows no detectable nucleic acid contamination (Figure S2D). There is a basal level of absorbance at 254 nm in the protein sample that increases significantly in the presence of added RNA (Figures S2C and S2E). A peak of around 40 mAU is observed for all samples around the 7 kDa molecular weight range. We do not expect this to be a co-purifying RNA based on the absorbance at 260 and 254 nm. To further exclude the possibility of fortuitous RNA contamination, we performed ^{32}P -labeling experiments to label any co-purified RNA (Figure S3). As shown in Figure S3A, the ^{32}P signal is only detectable when external RNA is added to the protein. A gel to show the minimal amount of RNA that can be detected by this method demonstrates that 5 ng RNA is detectable (Figure S3B). A molarity calculation based on the protein (1 mM) used in the labeling experiment, as well as the limit of RNA detection (1 ng), yielded an ~500:1 protein-to-RNA ratio, i.e., >99.8% of the protein molecules in our preparation are free of contaminating RNA. This is likely an overestimate of contamination by RNAs that could conceivably act as nuclease guides, because we are considering all RNAs regardless of their complementarity with the DNAs that we use as cleavage substrates. Therefore, we conclude that fortuitously contaminating RNAs, acting as conventional Cas9 or Cas12a guides, do not account for the Mn^{2+} -dependent DNA cleavage activities observed.

Active Site Requirements Vary for RNA-Independent DNA Cleavage Activities

To identify the active site contributions for RNA-independent DNA cleavage by SpyCas9, FnoCas9, and FnoCas12a, we performed the cleavage assays with wild-type and active site mutants of the respective proteins. Previous studies have shown that active site mutants fold similarly to wild-type and perform RNA-dependent DNA cleavage activity (Hirano et al., 2016; Jinek et al., 2012, 2014; Yamano et al., 2016). In the case of FnoCas9, the RNA-independent activity is abolished in the HNH-inactive single mutant and the HNH- and RuvC-inactive double mutant (Figure 3A). This implicates the FnoCas9 HNH domain in RNA-independent ds plasmid cleavage. SpyCas9 ssDNA degradation depends on the RuvC domain, because a RuvC-inactive mutant did not degrade circular ssDNA (Figure 3B). In the case of FnoCas12a, both the RuvC and the Nuc domains are essential for RNA-independent DNA cleavage, because mutations in either of the active sites failed to cleave the DNA (both

ssDNA and dsDNA) (Figures 3C and 3D). Our results recapitulate previous studies that showed that Cas9 RNA-dependent DNA cleavage is carried out by the independent activities of the endonuclease domains, while Cas12a requires a functional RuvC domain for its activity (Jinek et al., 2012; Swarts et al., 2017). Our mutational experiments also demonstrate that DNA cleavage activity is not attributable to a co-purified cellular nuclease, because one amino acid change may not abolish co-purification of a cellular nuclease.

RNA-Independent DNA Nickase Activity Is Non-sequence Specific

To analyze the sequence specificity of RNA-independent DNA cleavage, the products of RNA-dependent and RNA-independent cleavage by Cas proteins were subjected to restriction enzyme digestion. The rationale was that plasmids subjected to sequence-specific cleavage will lead to a definitive banding pattern after restriction digestion, whereas plasmids with nonspecific cleavage will not show specific banding patterns (Figure 4). Products were analyzed on native and alkaline (denaturing) agarose gels. The nicked products (two bands on alkaline gel: linear and closed circular) from RNA-independent cleavage are converted to linear bands upon restriction digestion, without accumulation of products of any specific size. For a comparison, specific bands are observable when an RNA-dependent product (linear) is treated with restriction enzymes.

RNA-Independent Activity Varies with Substrate Type

To determine the substrate selectivity and further analyze the DNA-sequence specificity of RNA-independent DNA cleavage activity, EcoRI-linearized pUC19 and EcoRI-linearized M13mp18 were used as substrates (Figures 5 and S4). While there is no prominent cleavage of linear dsDNA (Figures S4A and S4B), linear ssDNA is easily degraded by FnoCas12a and SpyCas9 and to a lesser extent by FnoCas9 (Figures 5A and 5B). A comparison with alkaline gel shows that both closed circular and linear single-stranded (ss) M13mp18 (due to incomplete linearization of M13mp18) are degraded by FnoCas12a and SpyCas9. Following this, we used a ³²P-labeled ss 60-mer-long oligonucleotide (oligo) as a substrate. Only FnoCas12a cleaved this DNA, showing that DNA modifications are not driving the DNA cleavage (Figures 5C and S4C). In the case of FnoCas12a, the cleavage product size does not correspond to that expected for PAM-dependent cleavage (Cas12a cleaves ~20 nt downstream of the PAM sequence) (Figure S4D) (Zetsche et al., 2015). SpyCas9 does not cleave the ss oligo despite the presence of PAM sequences in the oligo (Figure S4E). It is most likely that features other than PAM sequences contribute to defining sites of DNA cleavage. A ds 60-mer oligo does not produce visible products with any of the Cas proteins analyzed (Figure S4F). Our experiments do not rule out the possibility of DNA sequence- or structure-specific hotspots for the RNA-independent DNA cleavage. Further experiments involving deep sequencing approaches may reveal such hotspots. However, while informative, such evidence would support a sequence or structural preference rather than strict specificity.

Mn²⁺ Promotes Nickase Activity when Only One of the Two Cognate RNAs Is Available

We analyzed plasmid cleavage in the presence of one of the cognate RNAs (crRNA or tracrRNA) and its relation to the type of divalent metal ion present in the reaction. We found that in the presence of Mg²⁺, FnoCas9 is tightly regulated and linearizes the plasmid strictly

in the presence of both crRNA and tracrRNA (Figures 6A and 6B). Similarly, FnoCas12a, which requires only crRNA for RNA-dependent cleavage, linearizes the substrate plasmid only when crRNA and Mg^{2+} are present (Figure S5A). In the presence of Mn^{2+} , FnoCas9 nicks the plasmid in an RNA-independent manner if only one of the two RNAs (crRNA or tracrRNA) is present in the reaction, while it linearizes in an RNA-dependent manner when both crRNA and tracrRNA are available (Figure 6A). A comparison between the relative efficiencies of RNA-dependent (100%) and RNA-independent (50%–80%) activities can be seen in the reactions carried out with RNA- Mn^{2+} and Mn^{2+} (Figures 6A and S5). Accompanying experiments showed that in FnoCas9-D11A (in which the HNH domain is active), non-specific nicking can happen in the presence of Mn^{2+} and one of the two RNAs, while in the presence of both RNAs and Mn^{2+} , the nicking should be strand specific, as has been previously observed (Figure 6A) (Hirano et al., 2016; Jinek et al., 2012). An HNH-inactive mutant (FnoCas9-H969A) only possessed RNA-dependent, strand-specific nicking, while a double endonuclease mutant is inactive (Figure 6B). In the case of FnoCas12a, the Nuc domain mutant retained RNA-dependent nicking in the presence of Mn^{2+} , similar to previous observations with Mg^{2+} (Yamano et al., 2016), while the individual (RuvC or Nuc) active site mutants of FnoCas12a lost the RNA-independent activity in the presence of Mn^{2+} (Figure S5A). An experiment was conducted with a cognate substrate and a non-cognate substrate with FnoCas9 (Figure S5B) or FnoCas12a (Figure S5C) and Mn^{2+} . With a non-cognate substrate, RNA-independent activity is promoted in the presence of one or none of the cognate RNAs in FnoCas9 and in the absence of crRNA in FnoCas12a. When all required RNA components are present, the noncognate substrate is not cleaved, while the cognate substrate is linearized by FnoCas9 and FnoCas12a.

Metal Dependency for the RNA-Independent DNA Cleavage Activity

To determine whether the RNA-independent DNA cleavage occurs at lower Mn^{2+} concentrations, we performed the cleavage assays at varying metal concentrations (Figure S6). We observed ds plasmid nicking starting at 500 mM Mn^{2+} in the case of FnoCas9 and at only 10 mM in the case of FnoCas12a (Figures S6A and S6B). The ssDNA cleavage is more efficient at a lower Mn^{2+} concentration (250 mM for SpyCas9 and FnoCas12a) compared to dsDNA cleavage (Figures S6C and S6D). We proceeded to analyze the effect of two divalent metals in promoting RNA-independent DNA cleavage. The rationale was to test whether the presence of Mg^{2+} ions will abolish the Mn^{2+} -dependent, RNA-independent DNA cleavage activity. The RNA-independent activity was performed under three sets of conditions: 1, 5, and 10 mM Mn^{2+} . For each Mn^{2+} concentration, 0, 1, or 2 mM Mg^{2+} concentrations were tested. We did not detect Mg^{2+} inhibition of the Mn^{2+} -dependent activities under these conditions (Figures S6E–S6H).

To identify whether other divalent metals can promote the RNA-independent DNA cleavage activity, we performed an array of reactions using different divalent metals (Figure S7). The ds plasmid nicking activity is promoted by Co^{2+} in both FnoCas12a and FnoCas9, while metals such as Ni^{2+} , Cu^{2+} , and Zn^{2+} promoted a minimal level of activity in the case of FnoCas9 (Figures S7A and S7B). No ds plasmid nicking was observed for SpyCas9 using the different divalent metal ions tested in this study (Figure S7C). For circular ssDNA degradation, Co^{2+} promoted minimal activity in FnoCas12a and complete degradation in

SpyCas9 (Figures S7D and S7E). Some degradation was visible for SpyCas9 in the presence of 10 mM Ni²⁺ as well (Figure S7E). In the case of FnoCas9, Co²⁺ promoted ssDNA degradation (Figure S7F). The substitution of Mg²⁺ with other divalent metal ions was shown to be successful for RNA-dependent DNA cleavage in SpyCas9 (Ca²⁺, Mg²⁺, and Mn²⁺) (Jinek et al., 2012), FnoCas9 (Mg²⁺ and Zn²⁺) (Hirano et al., 2016), FnoCas12a (Ca²⁺, Mg²⁺, and Mn²⁺) (Zetsche et al., 2015), and *Neisseria meningitidis* Cas9 (Mg²⁺, Ca²⁺, and Ba²⁺) (Zhang et al., 2015). Our experiments show that Co²⁺ behaves identically to Mn²⁺ in promoting RNA-independent DNA cleavage in all Cas proteins tested. Certain protein-specific differences in the divalent metal requirement are visible for the RNA-independent activity (e.g., FnoCas12a activity is supported by only Mn²⁺ and Co²⁺, whereas FnoCas9 and SpyCas9 can accommodate several other divalent metal ions for this reaction).

Mn²⁺ and DNA Trigger Conformational Changes in Cas Proteins that Are Distinct from Apo- and RNA-Bound Forms of the Proteins

Several studies on SpyCas9 and Cas12a have shown that the apo protein binds to RNA to undergo large conformational changes essential for cleavage of target DNA (Gao et al., 2016; Jinek et al., 2014; Nishimasu et al., 2014; Swarts et al., 2017). We performed limited trypsin digestion of apo-, cognate RNA-bound, DNA-Mn²⁺-bound, and DNA-Mg²⁺-bound forms of the Cas proteins to probe their structural differences (Figure 7). In the case of SpyCas9, Mn²⁺-ssDNA- and Mn²⁺-dsDNA-bound Cas9 showed a comparable proteolytic digestion pattern to that of the single guide RNA (sgRNA)-SpyCas9 complex. The Mn²⁺-DNA-bound form produced a more stable conformation compared to that of the Mg²⁺-DNA-bound form. The full-length apo-SpyCas9 protein is digested into fragments by trypsin, whereas there is stabilization of the full-length protein in the RNA- and DNA-bound forms (Figure 7A). In the case of FnoCas9, the RNA-bound and DNA-bound forms (both ss and ds) had similar digestion patterns with both Mg²⁺ and Mn²⁺ conditions, and these conformations are different from the apo form (Figure 7B). For FnoCas12a, DNA-bound conformations are similar in the presence of both Mn²⁺ and Mg²⁺, and it is different from the apo form. In FnoCas12a, the DNA-bound forms possess a distinct banding pattern (e.g., ~37 kDa) that is absent in the apo- or RNA-bound forms of FnoCas12a (Figure 7C). Our experiments demonstrate that while RNA-bound conformational changes are essential for RNA-dependent DNA cleavage, DNA and Mn²⁺ can trigger conformational changes required for RNA-independent DNA cleavage by Cas9 and Cas12a.

DISCUSSION

Protein Conformation in Relation to RNA-Independent Activity

Several structural and biophysical studies have provided insight into the mechanism of activation of Cas9 and the basis of sequence-specific, RNA-guided DNA cleavage (Jinek et al., 2014; Nishimasu et al., 2014; Sternberg et al., 2015). In the absence of sgRNA, apo-SpyCas9 binds DNA in a sequence-independent manner with a binding affinity of 25 nM, in comparison to the SpyCas9-sgRNA complex binding complementary DNA with an affinity of 0.5 nM (Sternberg et al., 2014). The high-affinity non-specific DNA binding of apo-SpyCas9 in the absence of sgRNA shows that conditions exist that can promote RNA-independent activity. Structural or catalytic features are imparted by Mn²⁺ or Co²⁺ that

facilitate RNA-independent DNA cleavage by Cas proteins. In the case of RNA-dependent DNA cleavage by Cas9 and Cas12a, sequence specificity is based on RNA-DNA base-pairing and PAM recognition, followed by a ruler mechanism to locate the cleavage position, not by direct sequence recognition of the cleavage region. It is likely that the observed sequence-independent DNA cleavage in the absence of RNA is facilitated by conformational changes induced by the specific divalent metals. Such conformational changes may orient the endonuclease domain ideally for DNA cleavage.

Based on limited proteolysis patterns of SpyCas9 and FnoCas12a, we postulate that the active site assembly (positioning of the HNH and the RuvC domains) and the subsequent conformational changes occurring in the Cas9-DNA complex are not identical when compared to the Cas9-sgRNA complex (Figure 7). SpyCas9 showed differences between the Cas9-DNA-Mg²⁺ and Cas9-DNA-Mn²⁺ conformations. While sequence-specific sgRNA interaction with the bridge helix causes large re-arrangements in the REC domain of Cas9 during RNA-dependent DNA cleavage (Nishimasu et al., 2014), this may not occur in the case of the RNA-independent activity. Similarly, the conserved phosphate lock loop that is essential for R-loop formation in Cas9 and Cas12a orthologs may not be essential for RNA-independent activity (Murugan et al., 2017). The RNA-independent DNA cleavage may involve conformational changes that place the DNA close to the endonuclease site where DNA cleavage occurs.

The relative flexibilities of the HNH and RuvC domains vary. The HNH domain is highly flexible compared to the RuvC domain. The HNH domain of SpyCas9 is ordered in the various crystal structures of SpyCas9, with increased stabilization coming from RNA-DNA binding compared to the apo protein (Hirano et al., 2016; Jinek et al., 2014; Jiang et al., 2016; Nishimasu et al., 2014). In contrast, the electron density for HNH was weak in the crystal structure of FnoCas9 bound to the RNA-DNA hybrid, suggesting high mobility of this domain compared to the rest of the protein (Hirano et al., 2016). Even in the apo-SpyCas9 crystal structure, more regions of the HNH are visible compared to the FnoCas9-RNA-DNA-bound structure. In the recently reported CjeCas9 structure, the entire HNH domain had to be deleted to enable crystallization (Yamada et al., 2017). Altogether, these observations emphasize the differences in the flexibility of the HNH domain in different Cas9 orthologs, providing evidence for functional differences. A more mobile HNH domain may engage a dsDNA substrate non-specifically without a guide RNA and contribute to nicking by FnoCas9, but this may not be possible in the more rigid HNH domain of SpyCas9.

CRISPR-Cas9, CRISPR-Cascade, and Argonautes use similar mechanisms of target DNA binding to the pre-assembled RNP complex, even though they evolved divergently (Gao et al., 2016). Despite the mechanistic differences in RNA-dependent DNA cleavage, both Cas9 and Cas12a possess Mn²⁺-dependent, RNA-independent DNA cleavage activities. It was reported that Cas5d, the protein essential for metal-independent crRNA maturation in type I-C systems, possesses divalent metal-dependent DNase activity on a variety of DNA substrates (Punetha et al., 2014). Csd1, a component of the type I-C effector complex, also possesses RNase and metal-dependent DNA cleavage activities (Punetha et al., 2014). This

emphasizes the capabilities of Cas proteins of different CRISPR types in performing diverse DNA cleavage activities.

Contribution of Mn^{2+} to Diverse Activity in Other DNA-Metabolizing Enzymes

Several DNA-metabolizing enzymes exhibit differences in catalytic function based on the identity of the divalent metal involved in the reaction. For example, DNase I exhibits a higher level of activity and simultaneous cleavage of both strands of the DNA in the presence of Mn^{2+} compared to Mg^{2+} (Melgar and Goldthwait, 1968). Mn^{2+} and Co^{2+} ions have the unique ability to bind the DNA strand between a guanine base and an adjacent phosphate, producing a local unwinding effect on the DNA. The destabilized DNA is acted upon by multiple DNase I molecules, which is not achieved by metals such as Mg^{2+} , Ca^{2+} , and Zn^{2+} (Campbell and Jackson, 1980). In addition to changes in DNA structure, metal binding can promote conformational changes in the protein-DNA complex to position the scissile phosphate closer to the nucleophile in the active site.

Both Mn^{2+} and Co^{2+} have a preferred octahedral geometry, and they may bind to the protein, the DNA, or both in the complex. Even though Mg^{2+} can form an octahedral coordination sphere, Mn^{2+} and Co^{2+} may promote optimal orientation of the DNA in the active site to catalyze DNA cleavage in the absence of a guide RNA. This observation is supported by the crystal structures of DNA ligase D 3'-phosphoesterase (PE) enzyme, where Mn^{2+} and Co^{2+} promote a productive orientation of the metal, phosphate, and active site residues of the protein, but Zn^{2+} does not (Das et al., 2012). Many Mn^{2+} -dependent DNA repair enzymes are active specifically in the presence of Mn^{2+} , but not with Mg^{2+} (Das et al., 2012; Zhu and Shuman, 2005), because of reduced transition state stability in the presence of Mg^{2+} . In the case of DNA polymerases, divalent metal ions such as Mn^{2+} , Co^{2+} , Ni^{2+} , and Zn^{2+} can substitute for Mg^{2+} , with a subsequent reduction in fidelity and processivity of the enzyme (Frank and Woodgate, 2007). Some families of polymerases have evolved to use Mn^{2+} as the native co-factor, because Mn^{2+} promotes catalytic reactions that are not supported by Mg^{2+} ions due to the relaxed metal coordination and the active site flexibility that results from Mn^{2+} coordination (Frank and Woodgate, 2007; Yang et al., 2006). These observations can be applied to the RNA-independent DNA cleavage activities of Cas proteins. The presence of both cognate RNAs and Mn^{2+} leads to RNA-dependent activity, while the presence of one or none of the RNAs and Mn^{2+} leads to RNA-independent activity in FnoCas9, indicating the capabilities of Cas proteins to adopt different conformations based on the availability of RNA and divalent metals. Metal ions are not usually discernable within Cas9 structures, except in the case of FnoCas9, where a Zn^{2+} ion is essential for structural assembly of the REC3 domain, a region of the recognition lobe that is unique to FnoCas9 (Hirano et al., 2016). Thus, the observed differences in cleavage activity in the absence of RNA and in the presence of distinct divalent metals should not stem from drastic protein structural changes due to the absence of a structural Mg^{2+} ion.

Significance of RNA-Independent Activity in Genome Editing and Bacterial Physiology

Our experiments show that the RNA-independent DNA cleavage could occur at Mn^{2+} concentrations as low as 250 mM, especially in the case of ssDNA substrates. Mn^{2+} is essential for the survival of most organisms due to its role as an enzyme co-factor, ability to

provide protection during oxidative stress, contributions to transcriptional control mechanisms, and a host of other cellular roles (Jakubovics and Jenkinson, 2001). The effective physiological concentration of Mg^{2+} and Mn^{2+} varies considerably. For example, intracellular concentrations of Mg^{2+} can range from 2 to 3 mM of free Mg^{2+} up to 100 mM of bound Mg^{2+} in *Escherichia coli* (Cayley et al., 1991; Moncany and Kellenberger, 1981). Mn^{2+} can accumulate at millimolar concentrations in *E. coli* and many lactobacilli without deleterious effects to the cell (Jakubovics and Jenkinson, 2001; McEwan, 2009). The concentration of bound Mn^{2+} can differ from that of free Mn^{2+} , thus affecting the net available concentration of Mn^{2+} to any specific protein (Akabayov and Richardson, 2011). Thus, it is possible for Cas proteins to encounter effective Mn^{2+} concentrations required for RNA-independent DNA cleavage under cellular conditions.

This finding may have significant impacts on CRISPR-mediated genome editing and warrants further consideration. Our results show that in the presence of one of the cognate RNAs (tracrRNA or crRNA) and Mn^{2+} , RNA-independent activity is promoted in Cas9 orthologs, which may be important in sgRNA design. Our experiments also show that SpyCas9 is superior to both FnoCas9 and FnoCas12a for ds genome editing under a broader range of conditions due to the absence of RNA-independent ds plasmid nicking activity in SpyCas9 under all divalent metal concentrations tested. A previous study that monitored mice offspring for undesirable effects following prolonged Cas9 expression found no morphological abnormalities or evidence of increased DNA damage (Platt et al., 2014). This may be attributed to the relative dearth of ssDNA sites in the mouse genome; Mn^{2+} concentrations below the threshold for promoting the RNA-independent DNA cleavage; the co-expression of Cas9 and sgRNA, thereby limiting promiscuous activity; or any combination of these. One study reported a high occurrence of single-nucleotide variants in mice edited using CRISPR-Cas9 (Schaefer et al., 2017), though these findings require additional support. Nonetheless, these and other reports emphasize the importance of further characterization of CRISPR systems in development for human therapeutic applications.

Mn^{2+} is essential for virulence, pathogenicity, and sporulation in many bacteria (Jakubovics and Jenkinson, 2001). Under these conditions, we can postulate that the Mn^{2+} -dependent, RNA-independent DNA cleavage activity of Cas9 and Cas12a may play a role in bacterial pathogenesis by degrading or nicking DNA in a sequence-independent manner without a guide RNA. As one possible example, immune responses in many organisms, including humans and mice, involve secretion of extracellular traps (ETs) outside of the cell to prevent bacterial infection (Goldmann and Medina, 2013). ETs are composed of extensive DNA networks, along with antimicrobial proteins, and they have been shown to engulf bacteria that are ultimately killed by antimicrobial peptides in the trap (Brinkmann et al., 2004). Pathogens that were shown to escape ETs tend to possess powerful DNases that can cleave the backbone of an ET, thereby dismantling the antimicrobial peptides (Goldmann and Medina, 2013). In such a scenario, along with the importance of Mn^{2+} in some cases of bacterial virulence, it is conceivable that Cas9/Cas12a may promote non-specific DNA cleavage as a means of increasing bacterial pathogenicity. Previous studies have shown that Cas9 deletion mutants of *C. jejuni* and *N. meningitidis* had decreased virulence, lending weight to such hypotheses (Louwen et al., 2013; Sampson et al., 2013).

EXPERIMENTAL PROCEDURES

Detailed experimental and analytical procedures are presented in the Supplemental Information.

Bacterial Strains, Plasmids, and Oligonucleotides

The Fno genomic DNA was obtained from Biodefense and Emerging Infections Research Resources Repository (BEI Resources). The plasmids, oligonucleotides, and other resources used in the study are listed in the supplemental information (Tables S1–S4).

Cloning and Protein Purification

The Fno *cas9* and *cas12a* genes were cloned into a pET28a-based vector. Protein expression and purification of all the wild-type and mutant proteins followed previous protocols (Tables S2 and S3) (Jinek et al., 2012; Zetsche et al., 2015).

In Vitro Transcription

The transcription templates included DNA oligos (Table S4) or linearized plasmids containing the gene for the RNA of interest. The RNA was purified from an acrylamide-8 M urea gel.

Cleavage Assay

The cleavage assay using plasmids, linearized plasmids, and oligo DNAs was performed following previous protocols (Jinek et al., 2012). Control reactions include 10 mM Mn^{2+} and no protein. The quantification of activity is based on three replications of time course assays that used recombinant protein from different preparations. The gels were quantified using ImageJ (v.1.x) (Schneider et al., 2012). For the ds plasmid cleavage assays, the product formation was calculated using the formula $P = [N_i \div (SC_i + N_i)] \times 100$, where N_i represents the intensity of nicked DNA and SC_i represents the intensity of supercoiled DNA. The graphs were prepared by plotting the average cleavage from the three replications (P_{AV})

against the time points. SD was calculated using the formula $SD = \sqrt{\frac{\sum (P - P_{AV})^2}{(n - 1)}}$, and SEM was calculated using the formula $SD \div \sqrt{n}$, where n represents the number of replications. For circular ssDNA degradation, the intensity of the circular DNA remaining at each time point was measured and normalized before plotting over time using the formula $(CL_i \div CH_i) \times 100$, where CL_i is the intensity of circular DNA in each lane and CH_i is the highest intensity of circular DNA in each gel. SD and SEM were calculated using the same equations mentioned earlier, where P represents the non-degraded circular DNA.

UV-Visible Spectrophotometric Analysis of Cas Proteins

The absorbance at 254, 260, and 280 nm were recorded for SpyCas9, FnoCas9, and FnoCas12a proteins and RNP complexes while eluting out of an S200 increase column.

Quantification of Co-purified RNA

A ^{32}P labeling of RNA was performed with proteins and RNP complexes to detect trace amounts of co-purified RNA. The protein and RNP (a 1:1 molar ratio) samples were degraded by proteinase K, followed by phosphatase treatment (to remove the 5'-phosphate of RNAs), and labeling with ^{32}P .

Sequence Specificity Analysis

The cleavage products of RNA-dependent and RNA-independent reactions were subjected to restriction digestion, and the products were resolved on native and alkaline agarose gels (McDonnell et al., 1977).

Limited Trypsin Proteolysis

The wild-type SpyCas9, FnoCas9, and FnoCas12a proteins were treated with trypsin in their apo state, cognate RNA-bound state, or DNA-bound state, following previous protocols (Jiang et al., 2015; Ma et al., 2015).

Supplementary Material

Refer to Web version on PubMed Central for supplementary material.

Acknowledgments

We thank E. Sontheimer for critical discussions during the development of this manuscript. We thank L. Karr, A. West, G. Richter-Addo, and the Rajan lab members for helpful discussions. We acknowledge the OU Protein Production Core facility for protein purification services and instrument support and P. Bourne for help with absorbance measurements at multiple wavelengths. The OU PPC and the research in the R.R. lab are supported by an Institutional Development Award (IDeA) from the National Institute of General Medical Sciences of the NIH under grant P20GM103640.

References

- Akabayov B, Richardson CC. Binding of Mn-deoxyribonucleoside triphosphates to the active site of the DNA polymerase of bacteriophage T7. *Powder Diffr.* 2011; 26:159–162. [PubMed: 23761703]
- Barrangou R, Fremaux C, Deveau H, Richards M, Boyaval P, Moineau S, Romero DA, Horvath P. CRISPR provides acquired resistance against viruses in prokaryotes. *Science.* 2007; 315:1709–1712. [PubMed: 17379808]
- Brinkmann V, Reichard U, Goosmann C, Fauler B, Uhlemann Y, Weiss DS, Weinrauch Y, Zychlinsky A. Neutrophil extracellular traps kill bacteria. *Science.* 2004; 303:1532–1535. [PubMed: 15001782]
- Brouns SJ, Jore MM, Lundgren M, Westra ER, Slijkhuis RJ, Snijders AP, Dickman MJ, Makarova KS, Koonin EV, van der Oost J. Small CRISPR RNAs guide antiviral defense in prokaryotes. *Science.* 2008; 321:960–964. [PubMed: 18703739]
- Campbell VW, Jackson DA. The effect of divalent cations on the mode of action of DNase I. The initial reaction products produced from covalently closed circular DNA. *J. Biol. Chem.* 1980; 255:3726–3735. [PubMed: 6245089]
- Cayley S, Lewis BA, Guttman HJ, Record MT Jr. Characterization of the cytoplasm of *Escherichia coli* K-12 as a function of external osmolarity. Implications for protein-DNA interactions in vivo. *J. Mol. Biol.* 1991; 222:281–300. [PubMed: 1960728]
- Cong L, Ran FA, Cox D, Lin S, Barretto R, Habib N, Hsu PD, Wu X, Jiang W, Marraffini LA, Zhang F. Multiplex genome engineering using CRISPR/Cas systems. *Science.* 2013; 339:819–823. [PubMed: 23287718]

- Das U, Smith P, Shuman S. Structural insights to the metal specificity of an archaeal member of the LigD 3'-phosphoesterase DNA repair enzyme family. *Nucleic Acids Res.* 2012; 40:828–836. [PubMed: 21965539]
- Dong D, Ren K, Qiu X, Zheng J, Guo M, Guan X, Liu H, Li N, Zhang B, Yang D, et al. The crystal structure of Cpf1 in complex with CRISPR RNA. *Nature.* 2016; 532:522–526. [PubMed: 27096363]
- Fonfara I, Richter H, Bratovič M, Le Rhun A, Charpentier E. The CRISPR-associated DNA-cleaving enzyme Cpf1 also processes precursor CRISPR RNA. *Nature.* 2016; 532:517–521. [PubMed: 27096362]
- Frank EG, Woodgate R. Increased catalytic activity and altered fidelity of human DNA polymerase β in the presence of manganese. *J. Biol. Chem.* 2007; 282:24689–24696. [PubMed: 17609217]
- Gao P, Yang H, Rajashankar KR, Huang Z, Patel DJ. Type V CRISPR-Cas Cpf1 endonuclease employs a unique mechanism for crRNA-mediated target DNA recognition. *Cell Res.* 2016; 26:901–913. [PubMed: 27444870]
- Garneau JE, Dupuis ME, Villion M, Romero DA, Barrangou R, Boyaval P, Fremaux C, Horvath P, Magadán AH, Moineau S. The CRISPR/Cas bacterial immune system cleaves bacteriophage and plasmid DNA. *Nature.* 2010; 468:67–71. [PubMed: 21048762]
- Gasiunas G, Barrangou R, Horvath P, Siksnys V. Cas9-crRNA ribonucleoprotein complex mediates specific DNA cleavage for adaptive immunity in bacteria. *Proc. Natl. Acad. Sci. USA.* 2012; 109:E2579–E2586. [PubMed: 22949671]
- Goldmann O, Medina E. The expanding world of extracellular traps: not only neutrophils but much more. *Front. Immunol.* 2013; 3:420. [PubMed: 23335924]
- Hale CR, Zhao P, Olson S, Duff MO, Graveley BR, Wells L, Terns RM, Terns MP. RNA-guided RNA cleavage by a CRISPR RNA-Cas protein complex. *Cell.* 2009; 139:945–956. [PubMed: 19945378]
- Hirano H, Gootenberg JS, Horii T, Abudayyeh OO, Kimura M, Hsu PD, Nakane T, Ishitani R, Hatada I, Zhang F, et al. Structure and engineering of *Francisella novicida* Cas9. *Cell.* 2016; 164:950–961. [PubMed: 26875867]
- Ishino Y, Shinagawa H, Makino K, Amemura M, Nakata A. Nucleotide sequence of the iap gene, responsible for alkaline phosphatase isozyme conversion in *Escherichia coli*, and identification of the gene product. *J. Bacteriol.* 1987; 169:5429–5433. [PubMed: 3316184]
- Jakubovics NS, Jenkinson HF. Out of the iron age: new insights into the critical role of manganese homeostasis in bacteria. *Microbiology.* 2001; 147:1709–1718. [PubMed: 11429449]
- Jansen R, Embden JD, Gaastra W, Schouls LM. Identification of genes that are associated with DNA repeats in prokaryotes. *Mol. Microbiol.* 2002; 43:1565–1575. [PubMed: 11952905]
- Jiang F, Zhou K, Ma L, Gressel S, Doudna JA. Structural Biology. A Cas9-guide RNA complex preorganized for target DNA recognition. *Science.* 2015; 348:1477–1481. [PubMed: 26113724]
- Jiang F, Taylor DW, Chen JS, Kornfeldt JE, Zhou K, Thompson AJ, Nogales E, Doudna JA. Structures of a CRISPR-Cas9 R-loop complex primed for DNA cleavage. *Science.* 2016; 351:867–871. [PubMed: 26841432]
- Jinek M, Chylinski K, Fonfara I, Hauer M, Doudna JA, Charpentier E. A programmable dual-RNA-guided DNA endonuclease in adaptive bacterial immunity. *Science.* 2012; 337:816–821. [PubMed: 22745249]
- Jinek M, East A, Cheng A, Lin S, Ma E, Doudna J. RNA-programmed genome editing in human cells. *eLife.* 2013; 2:e00471. [PubMed: 23386978]
- Jinek M, Jiang F, Taylor DW, Sternberg SH, Kaya E, Ma E, Anders C, Hauer M, Zhou K, Lin S, et al. Structures of Cas9 endonucleases reveal RNA-mediated conformational activation. *Science.* 2014; 343:1247997. [PubMed: 24505130]
- Kamble VA, Misra HS. The SbcCD complex of *Deinococcus radiodurans* contributes to radioresistance and DNA strand break repair in vivo and exhibits Mre11-Rad50 type activity in vitro. *DNA Repair (Amst.).* 2010; 9:488–494. [PubMed: 20144564]
- Koonin EV, Makarova KS, Zhang F. Diversity, classification and evolution of CRISPR-Cas systems. *Curr. Opin. Microbiol.* 2017; 37:67–78. [PubMed: 28605718]
- Louwen R, Horst-Krefit D, de Boer AG, van der Graaf L, de Knecht G, Hamersma M, Heikema AP, Timms AR, Jacobs BC, Wagenaar JA, et al. A novel link between *Campylobacter jejuni*

- bacteriophage defence, virulence and Guillain-Barré syndrome. *Eur. J. Clin. Microbiol. Infect. Dis.* 2013; 32:207–226. [PubMed: 22945471]
- Ma E, Harrington LB, O'Connell MR, Zhou K, Doudna JA. Single-stranded DNA cleavage by divergent CRISPR-Cas9 enzymes. *Mol. Cell.* 2015; 60:398–407. [PubMed: 26545076]
- Mali P, Yang L, Esvelt KM, Aach J, Guell M, DiCarlo JE, Norville JE, Church GM. RNA-guided human genome engineering via Cas9. *Science.* 2013; 339:823–826. [PubMed: 23287722]
- Marraffini LA, Sontheimer EJ. CRISPR interference limits horizontal gene transfer in staphylococci by targeting DNA. *Science.* 2008; 322:1843–1845. [PubMed: 19095942]
- Marraffini LA, Sontheimer EJ. CRISPR interference: RNA-directed adaptive immunity in bacteria and archaea. *Nat. Rev. Genet.* 2010; 11:181–190. [PubMed: 20125085]
- McDonell MW, Simon MN, Studier FW. Analysis of restriction fragments of T7 DNA and determination of molecular weights by electrophoresis in neutral and alkaline gels. *J. Mol. Biol.* 1977; 110:119–146. [PubMed: 845942]
- McEwan AG. New insights into the protective effect of manganese against oxidative stress. *Mol. Microbiol.* 2009; 72:812–814. [PubMed: 19400770]
- Melgar E, Goldthwait DA. Deoxyribonucleic acid nucleases. II. The effects of metals on the mechanism of action of deoxyribonuclease I. *J. Biol. Chem.* 1968; 243:4409–4416. [PubMed: 5683998]
- Mojica FJ, Díez-Villaseñor C, García-Martínez J, Soria E. Intervening sequences of regularly spaced prokaryotic repeats derive from foreign genetic elements. *J. Mol. Evol.* 2005; 60:174–182. [PubMed: 15791728]
- Mojica FJM, Díez-Villaseñor C, García-Martínez J, Almendros C. Short motif sequences determine the targets of the prokaryotic CRISPR defence system. *Microbiology.* 2009; 155:733–740. [PubMed: 19246744]
- Moncany ML, Kellenberger E. High magnesium content of *Escherichia coli* B. *Experientia.* 1981; 37:846–847. [PubMed: 7026272]
- Murugan K, Babu K, Sundaresan R, Rajan R, Sashital DG. The revolution continues: newly discovered systems expand the CRISPR-Cas toolkit. *Mol. Cell.* 2017; 68:15–25. [PubMed: 28985502]
- Nishimasu H, Ran FA, Hsu PD, Konermann S, Shehata SI, Dohmae N, Ishitani R, Zhang F, Nureki O. Crystal structure of Cas9 in complex with guide RNA and target DNA. *Cell.* 2014; 156:935–949. [PubMed: 24529477]
- Nishimasu H, Cong L, Yan WX, Ran FA, Zetsche B, Li Y, Kurabayashi A, Ishitani R, Zhang F, Nureki O. Crystal structure of *Staphylococcus aureus* Cas9. *Cell.* 2015; 162:1113–1126. [PubMed: 26317473]
- Platt RJ, Chen S, Zhou Y, Yim MJ, Swiech L, Kempton HR, Dahlman JE, Parnas O, Eisenhaure TM, Jovanovic M, et al. CRISPR-Cas9 knockin mice for genome editing and cancer modeling. *Cell.* 2014; 159:440–455. [PubMed: 25263330]
- Punetha A, Sivathanu R, Anand B. Active site plasticity enables metal-dependent tuning of Cas5d nuclease activity in CRISPR-Cas type I-C system. *Nucleic Acids Res.* 2014; 42:3846–3856. [PubMed: 24371266]
- Sampson TR, Saroj SD, Llewellyn AC, Tzeng YL, Weiss DS. A CRISPR/Cas system mediates bacterial innate immune evasion and virulence. *Nature.* 2013; 497:254–257. [PubMed: 23584588]
- Schaefer KA, Wu WH, Colgan DF, Tsang SH, Bassuk AG, Mahajan VB. Unexpected mutations after CRISPR-Cas9 editing in vivo. *Nat. Methods.* 2017; 14:547–548. [PubMed: 28557981]
- Schneider CA, Rasband WS, Eliceiri KW. NIH Image to ImageJ: 25 years of image analysis. *Nat. Methods.* 2012; 9:671–675. [PubMed: 22930834]
- Sternberg SH, Redding S, Jinek M, Greene EC, Doudna JA. DNA interrogation by the CRISPR RNA-guided endonuclease Cas9. *Nature.* 2014; 507:62–67. [PubMed: 24476820]
- Sternberg SH, LaFrance B, Kaplan M, Doudna JA. Conformational control of DNA target cleavage by CRISPR-Cas9. *Nature.* 2015; 527:110–113. [PubMed: 26524520]
- Swarts DC, van der Oost J, Jinek M. Structural basis for guide RNA processing and seed-dependent DNA targeting by CRISPR-Cas12a. *Mol. Cell.* 2017; 66:221–233. [PubMed: 28431230]

- Wang H, Yang H, Shivalila CS, Dawlaty MM, Cheng AW, Zhang F, Jaenisch R. One-step generation of mice carrying mutations in multiple genes by CRISPR/Cas-mediated genome engineering. *Cell*. 2013; 153:910–918. [PubMed: 23643243]
- Wright AV, Nuñez JK, Doudna JA. Biology and applications of CRISPR systems: harnessing nature's toolbox for genome engineering. *Cell*. 2016; 164:29–44. [PubMed: 26771484]
- Yamada M, Watanabe Y, Gootenberg JS, Hirano H, Ran FA, Nakane T, Ishitani R, Zhang F, Nishimasu H, Nureki O. Crystal structure of the minimal Cas9 from *Campylobacter jejuni* reveals the molecular diversity in the CRISPR-Cas9 systems. *Mol. Cell*. 2017; 65:1109–1121. [PubMed: 28306506]
- Yamano T, Nishimasu H, Zetsche B, Hirano H, Slaymaker IM, Li Y, Fedorova I, Nakane T, Makarova KS, Koonin EV, et al. Crystal structure of Cpf1 in complex with guide RNA and target DNA. *Cell*. 2016; 165:949–962. [PubMed: 27114038]
- Yang W, Lee JY, Nowotny M. Making and breaking nucleic acids: two-Mg²⁺-ion catalysis and substrate specificity. *Mol. Cell*. 2006; 22:5–13. [PubMed: 16600865]
- Zetsche B, Gootenberg JS, Abudayyeh OO, Slaymaker IM, Makarova KS, Essletzbichler P, Volz SE, Joung J, van der Oost J, Regev A, et al. Cpf1 is a single RNA-guided endonuclease of a class 2 CRISPR-Cas system. *Cell*. 2015; 163:759–771. [PubMed: 26422227]
- Zhang Y, Rajan R, Seifert HS, Mondragón A, Sontheimer EJ. DNase H activity of *Neisseria meningitidis* Cas9. *Mol. Cell*. 2015; 60:242–255. [PubMed: 26474066]
- Zhu H, Shuman S. A primer-dependent polymerase function of *Pseudomonas aeruginosa* ATP-dependent DNA ligase (LigD). *J. Biol. Chem*. 2005; 280:418–427. [PubMed: 15520014]

Highlights

- FnoCas9, SpyCas9, and FnoCas12a cleave DNA without a gRNA in the presence of Mn^{2+}
- FnoCas9 nicks ds plasmid, while SpyCas9 degrades ssDNA
- FnoCas12a nicks ds plasmid and degrades ssDNA
- RNA-independent DNA cleavage appears not to be sequence specific

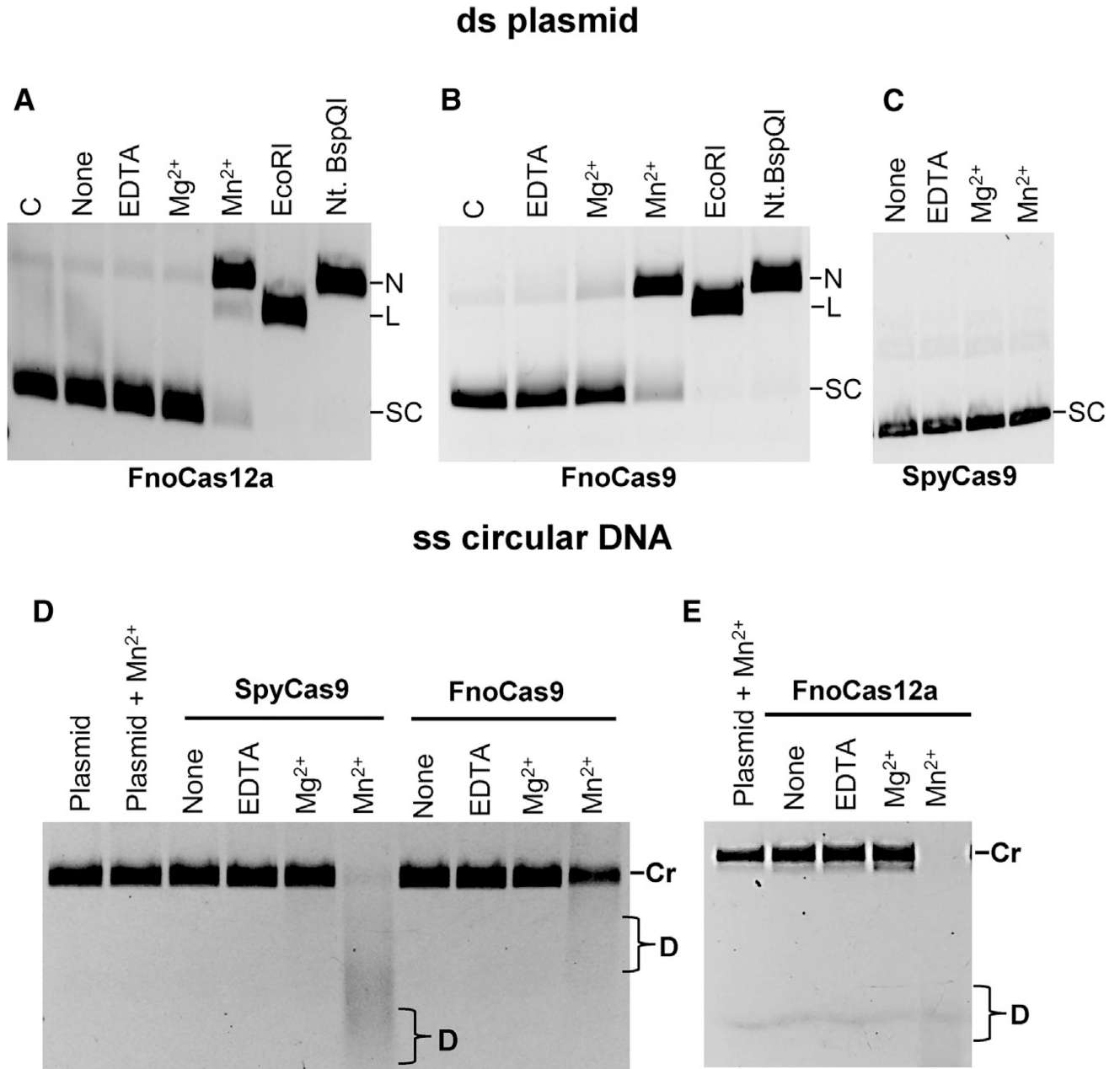


Figure 1. FnoCas9 and FnoCas12a Possess RNA-Independent dsDNA Nickase Activity while SpyCas9 and FnoCas12a Possess RNA-Independent ssDNA Degradation in the Presence of Mn²⁺

(A) dsDNA cleavage by FnoCas12a.

(B) dsDNA cleavage by FnoCas9.

(C) dsDNA cleavage by SpyCas9. FnoCas9 and FnoCas12a nicked pUC19 (ds plasmid) in the presence of Mn²⁺. There is limited linearization of the plasmid by FnoCas12a. For comparison, pUC19 was digested with EcoRI (linearizes [L]) or Nt.BspQI (nicks [N]). SpyCas9 does not nick or linearize pUC19.

(D) ssDNA cleavage by SpyCas9 and FnoCas9.

(E) ssDNA cleavage by FnoCas12a. M13mp18 circular (Cr) ssDNA was degraded by SpyCas9 and FnoCas12a in the presence of Mn²⁺. In comparison, FnoCas9 has limited

ssDNA degradation. D, degradation; C, control condition with no protein; None, condition with protein but no external metal or EDTA; SC, supercoiled. See also Figures S1–S3, S6, and S7.

Author Manuscript

Author Manuscript

Author Manuscript

Author Manuscript

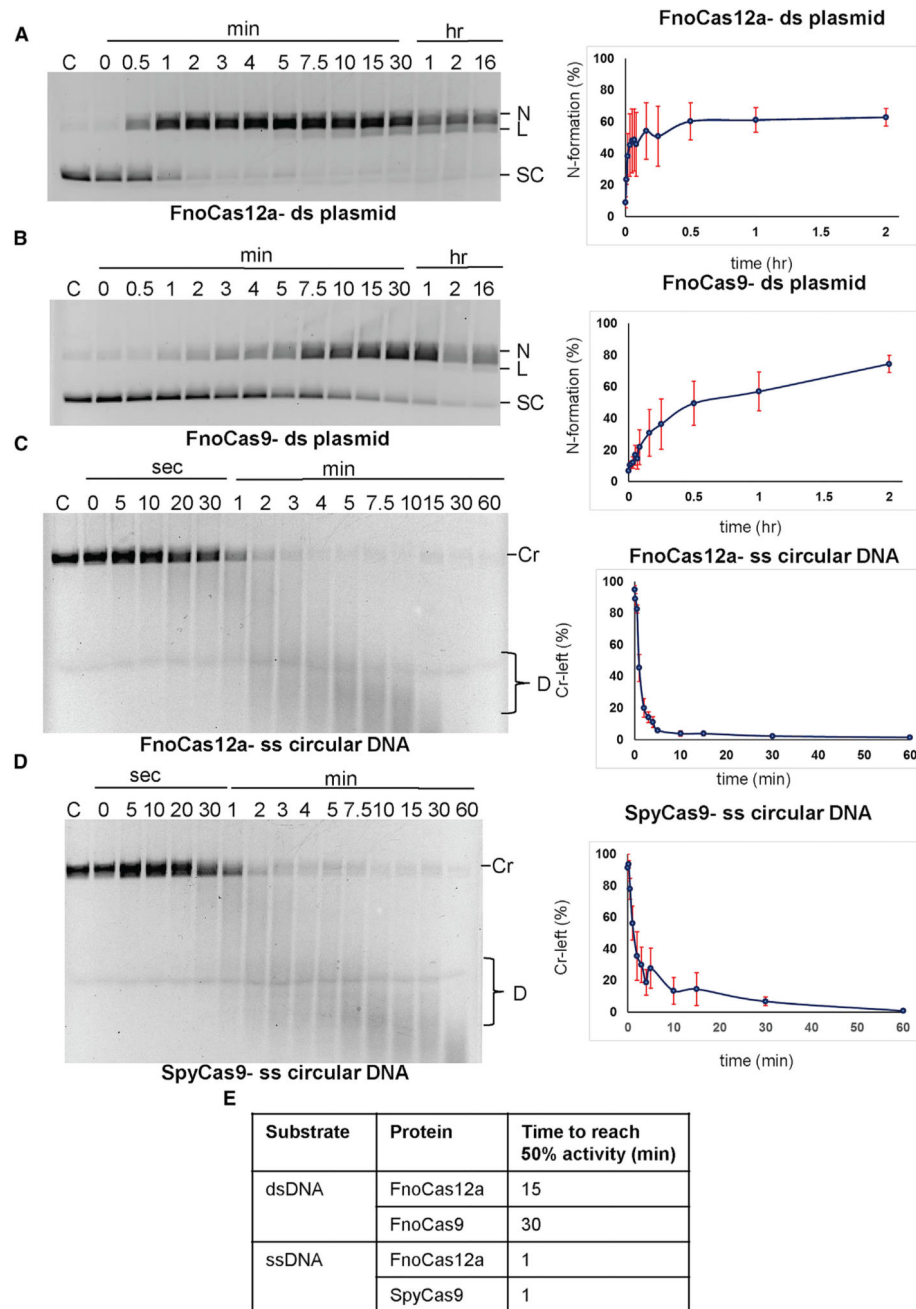


Figure 2. Time Course Assay to Quantify the RNA-Independent DNA Cleavage Activity
 (A) Activity of FnoCas12a on pUC19 plasmid. The major product is the nicked band. The linearization of the plasmid is incomplete after an overnight incubation.
 (B) Activity of FnoCas9 on pUC19 plasmid. The linearization of the plasmid is minimal compared to FnoCas12a.
 (C) Activity of FnoCas12a on M13mp18 circular DNA. The DNA is degraded, and there is no accumulation of lower molecular weight species except for the smaller degradation products.

(D) Activity of SpyCas9 on M13mp18 circular DNA. The DNA is degraded during the reaction. The graphs represent the average formation of nicked DNA for ds plasmid substrate or the amount of circular DNA left for circular ssDNA substrate. The graphs (mean \pm SEM) indicate activity based on quantification of DNA bands (Schneider et al., 2012), and error bars are from three replications performed using proteins from different protein preparations.

(E) Time to reach 50% activity for all activities.

The error bars are represented as SEM and were calculated using the formula

$SEM = SD / \sqrt{n}$, where n represents the number of replications (see Experimental

Procedures). SD was calculated using the formula $SD = \sqrt{\frac{\sum (P - P_{AV})^2}{(n - 1)}}$. C, control with no protein; N, nicked; L, linear; SC, supercoiled; Cr, circular ssDNA; D, degradation.

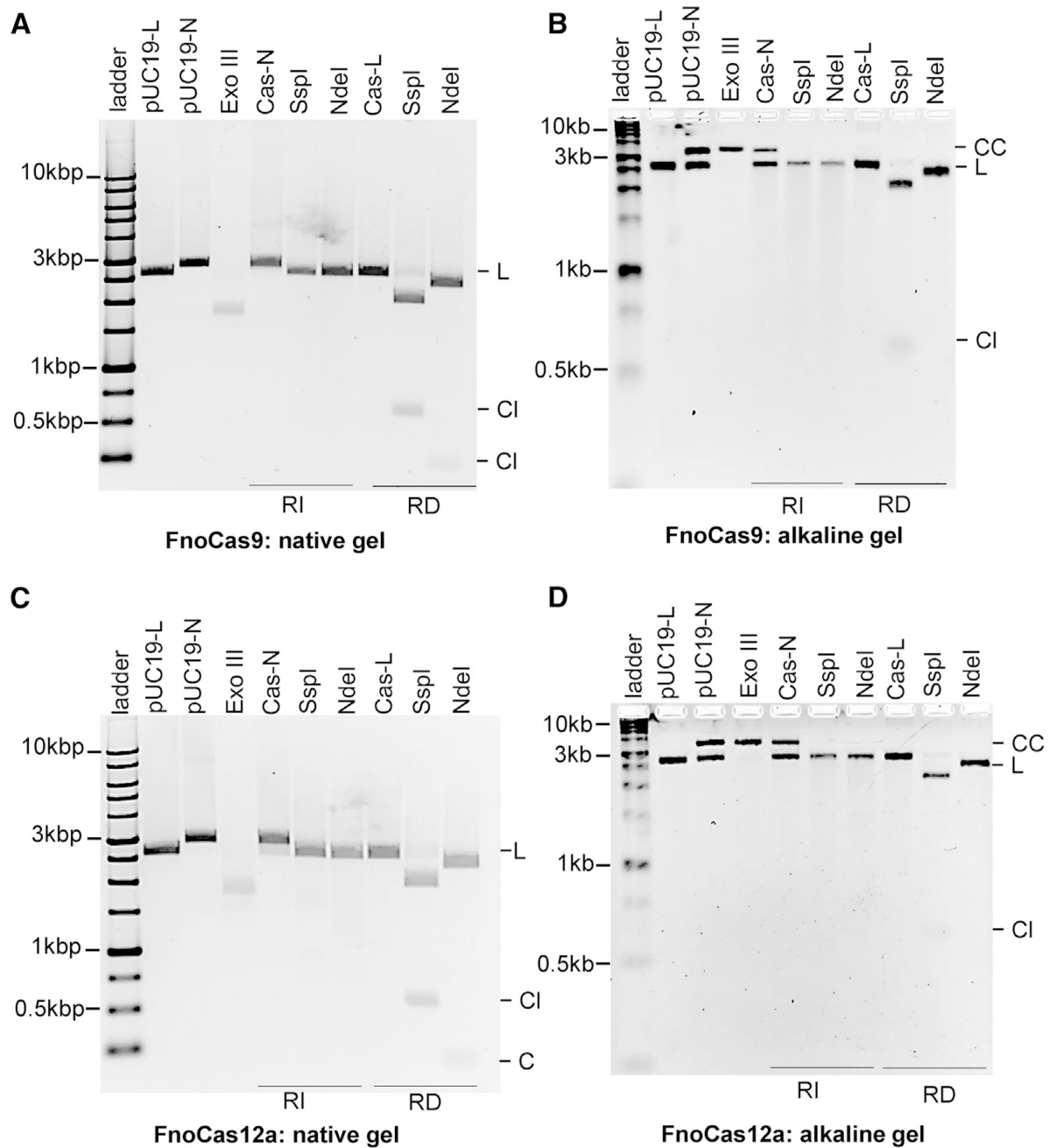


Figure 4. RNA-Independent DNA Nicking Activity by FnoCas9 and FnoCas12a Is Non-sequence Specific

(A and B) Restriction enzyme (RE) analysis of the cleavage products produced by FnoCas9 on a native agarose gel (A) and on a denaturing alkaline agarose gel (B).

(C and D) RE analysis of the cleavage products produced by FnoCas12a on a native agarose gel (C) and on a denaturing alkaline agarose gel (D). Comparison of native and alkaline gels shows that the nicked band produced by RNA-independent cleavage is converted to the linear product after RE digestion. The absence of specific-sized products compared to the lanes with RNA-dependent cleavage product analysis indicates that RNA-independent

activity is non-sequence specific. Identification of sequence- or structure-specific hotspots in the RNA-independent DNA cleavage will require further experiments.

pUC19-L, pUC19 treated with EcoRI; pUC19-N, pUC19 treated with Nt.BspQI; ExoIII: nicked pUC19 treated with exonuclease III, Exo III degrades linear DNA; Cas-N, nicked product from the RNA-independent activity of Cas protein (FnoCas9 or FnoCas12a); Cas-L, linear product from the RNA-dependent activity of Cas protein (FnoCas9 or FnoCas12a); L, linearization by RE; Cl, shorter cleavage product produced by sequence-specific digestion by RE; CC, closed circular; kbp, kilo base pairs; kb, kilobases; RI, RNA-independent cleavage; RD, RNA-dependent cleavage.

Author Manuscript

Author Manuscript

Author Manuscript

Author Manuscript

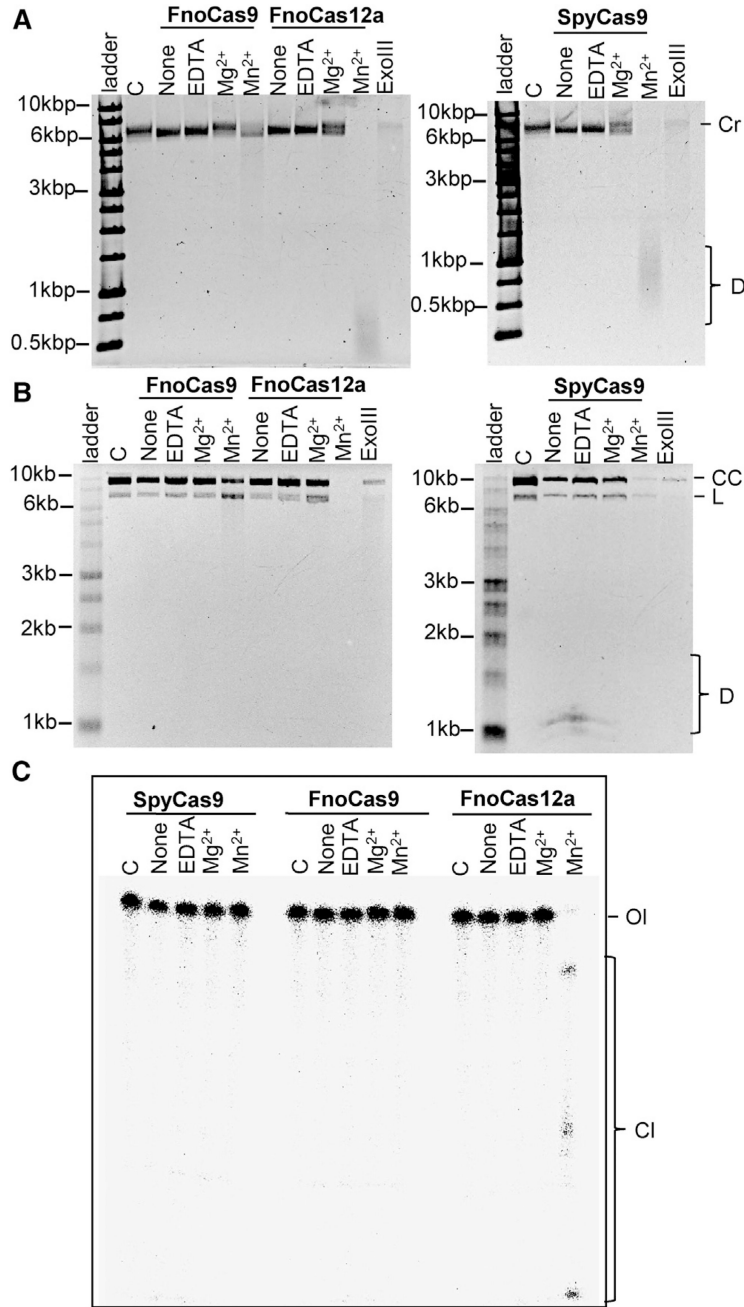


Figure 5. RNA-Independent DNA Nicking Activity on Linear DNA Substrates

(A and B) M13mp18 digested using EcoRI (one site) was treated with Cas proteins, and the products were analyzed on a native agarose gel (A) and a denaturing alkaline gel (B). Both FnoCas12a and SpyCas9 cleave linear ssDNA, while FnoCas9 has limited activity. The cleavage of M13mp18 with EcoRI is not complete, as seen by the presence of both closed circular (CC) and linear (L) bands on an alkaline gel. Exonuclease III (ExoIII) that degrades linear DNA is included to distinguish CC and L bands. Both CC and L DNA are degraded by FnoCas12a and SpyCas9.

(C) 5'-³²P-labeled ss oligo DNA was treated with Cas proteins. Only FnoCas12a cleaves ss oligo substrates.

C, control with no protein; none, reaction with protein without added metal; Cr, circular ss M13mp18; D, degradation; kbp, kilo base pairs; kb, kilobases; OI, 60-mer ss oligo; CI, cleavage products. See also Figure S4.

Author Manuscript

Author Manuscript

Author Manuscript

Author Manuscript

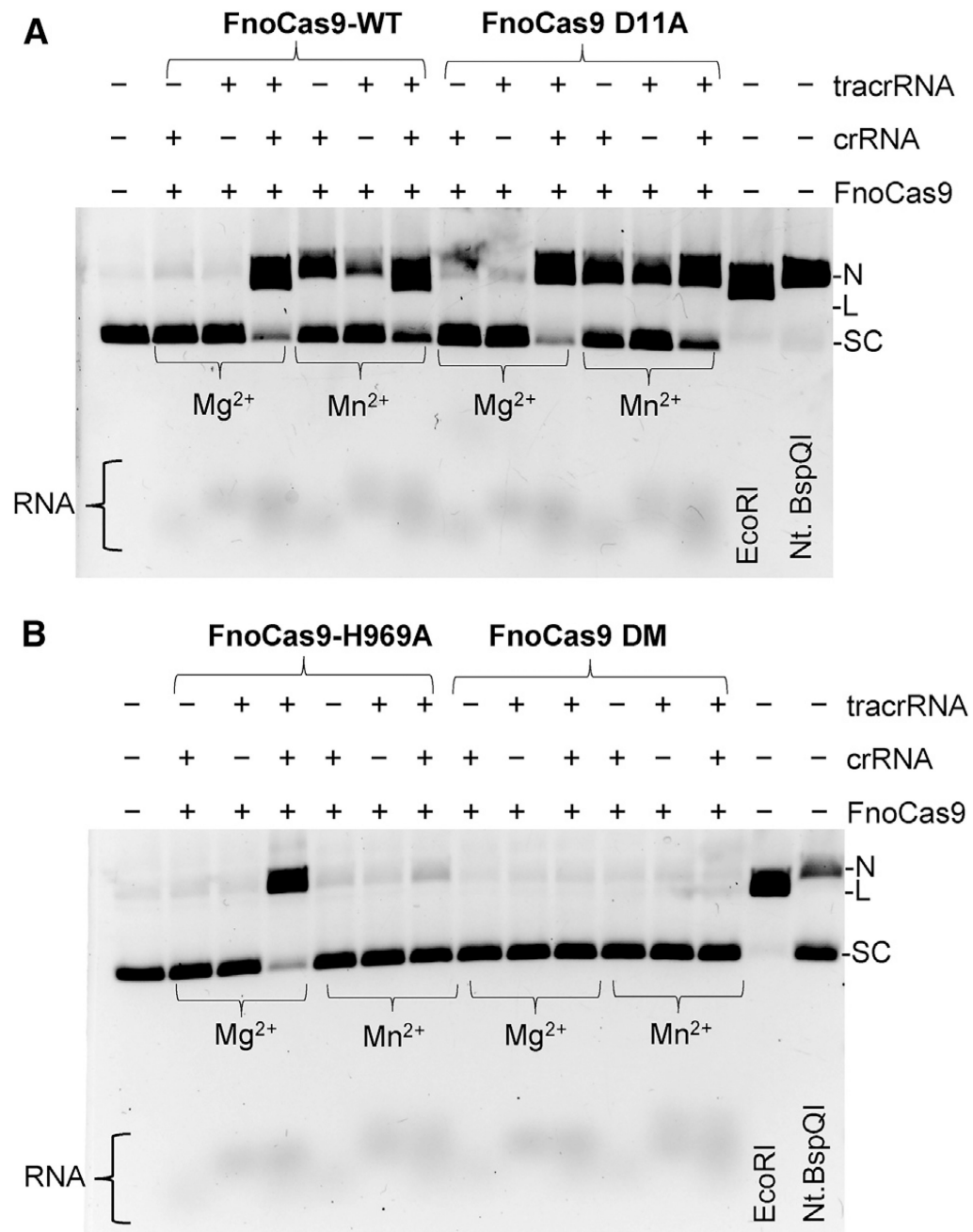


Figure 6. In the Presence of Either of the RNAs (crRNA or tracrRNA), Mn^{2+} Promotes RNA-Independent Activity by FnoCas9

(A) Activity of FnoCas9 wild-type (WT) and the RuvC-inactive (D11A) mutant.

(B) Activity of the FnoCas9 HNH-inactive (H969A) mutant and the double mutant (DM), where both RuvC and HNH are inactivated.

While Mg^{2+} promotes RNA-dependent DNA cleavage (linear product) only when both crRNA and tracrRNA are present in the reaction, Mn^{2+} can promote plasmid nicking when either crRNA or tracrRNA is present in the reaction and linearization when both RNAs are present. In the case of D11A, nicking is observed for RNA-dependent (both RNAs present) and RNA-independent activities. The mutants H969A and DM show negligible RNA-

independent activity. Control lanes with linear (L) bands produced by EcoRI digestion and nicked plasmids (N) produced by Nt.BspQI digestion are also shown. SC, supercoiled.

Author Manuscript

Author Manuscript

Author Manuscript

Author Manuscript

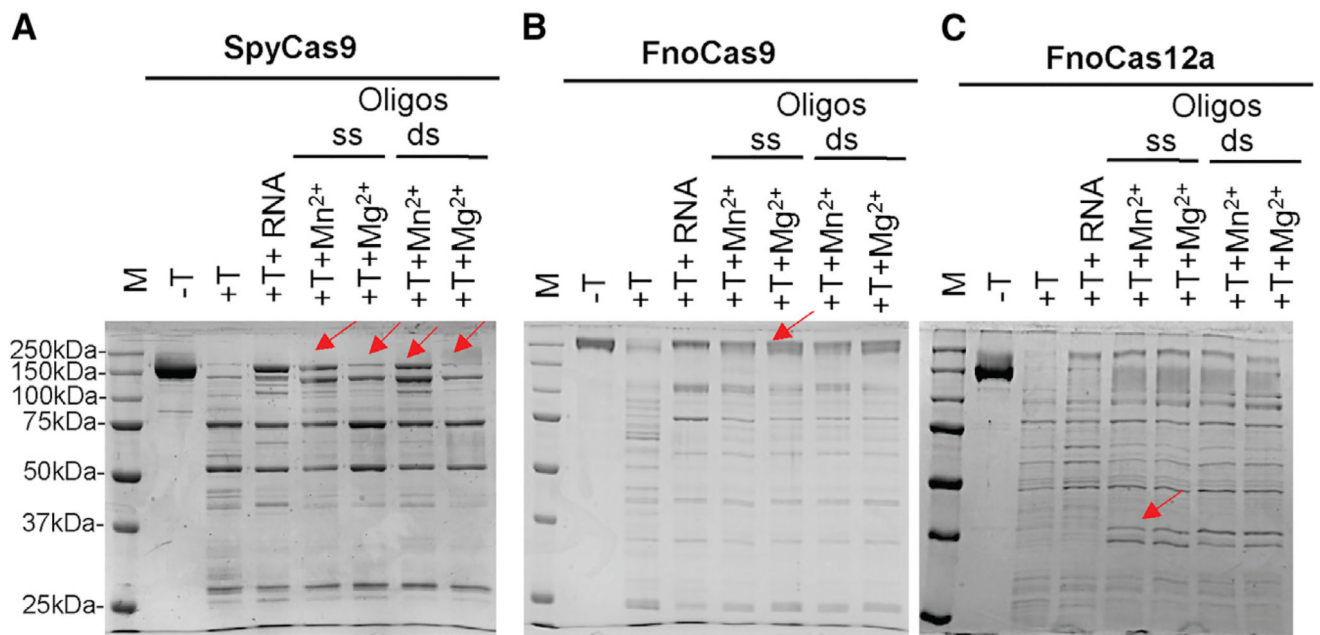


Figure 7. Limited Trypsin Proteolysis Suggests Structural Differences between Apo-, RNA-Bound, and DNA-Bound Forms of SpyCas9, FnoCas9, and FnoCas12a

(A) Limited proteolysis of SpyCas9. In the presence of Mn²⁺-DNA, full-length protein is more intact compared to Mg²⁺ (arrows).

(B) Limited proteolysis of FnoCas9. There are no visible differences between Mn²⁺ and Mg²⁺ digestion patterns (arrow).

(C) Limited proteolysis of FnoCas12a. A distinct pattern with additional bands at 37 kDa (arrow) is present for DNA-bound structures when compared to apo- and RNA-bound FnoCas12a.

For all proteins, apo protein is rapidly degraded, while the RNA- and DNA-bound structures appear to be more stable, with distinct banding patterns compared to apo protein digestion.

A protein marker (M) is present in each gel. T, trypsin.